Supporting Information

Dual Resistance and Impedance Investigation: Ultrasensitive and Stable Humidity Detection of Molybdenum Disulfide Nanosheets-Polyethylene Oxide Hybrids

Yanjie Wang[a], Yong Zhou*[a], Guangzhong Xie[b], Jing Li[a], Yuhang Wang[a], Xiaoyu Liu[c], Zhigang Zang[a]

[a]*Key Laboratory of Optoelectronic Technology and System of Ministry of Education, College of Optoelectronic Engineering, Chongqing University, Chongqing 400044, PR China*

[b]*State Key Laboratory of Electronic Thin Films and Integrated Devices, School of Optoelectronic Science and Engineering, University of Electronic Science and Technology of China (UESTC), Chengdu 610054, PR China*

[c]*Chongqing University Cancer Hospital, Chongqing University, Chongqing 400030, PR China*

* Corresponding author.

E-mail Address: zhyf@cqu.edu.cn (Y. Zhou).

Characterization Techniques

The thickness of MoS_2 flakes was probed via atomic force microscopy (AFM) in tapping mode. Zeta potential was calculated from Zeta potentiometer (Omni, BRUKE, USA). The surface wetting tests were executed with Rame-Hart USA water contact angle measurement unit equipment with CCD camera. Morphological images were gathered by scanning electron microscope (SEM, ZEISS, Evo18, Germany) operated at acceleration voltage of 5 kV. The surface area and pore size distribution was determined by using TriStar Ⅱ 3020 BET surface area analyser supplied by Micromeritics, USA. Fourier transform infrared spectroscopy (FTIR) was conducted by Shimadzu 8400S instrument system. X-ray diffraction spectra (XRD) was obtained by PANalytical X'pert HighScore XRD instrument with a CuKα radiation source. X-ray photoelectron spectroscopy (XPS) measurements were performed on an Omicron Nanotech operated at 15 kV and 20 mA current using monochromatic Al Kα X-ray source.

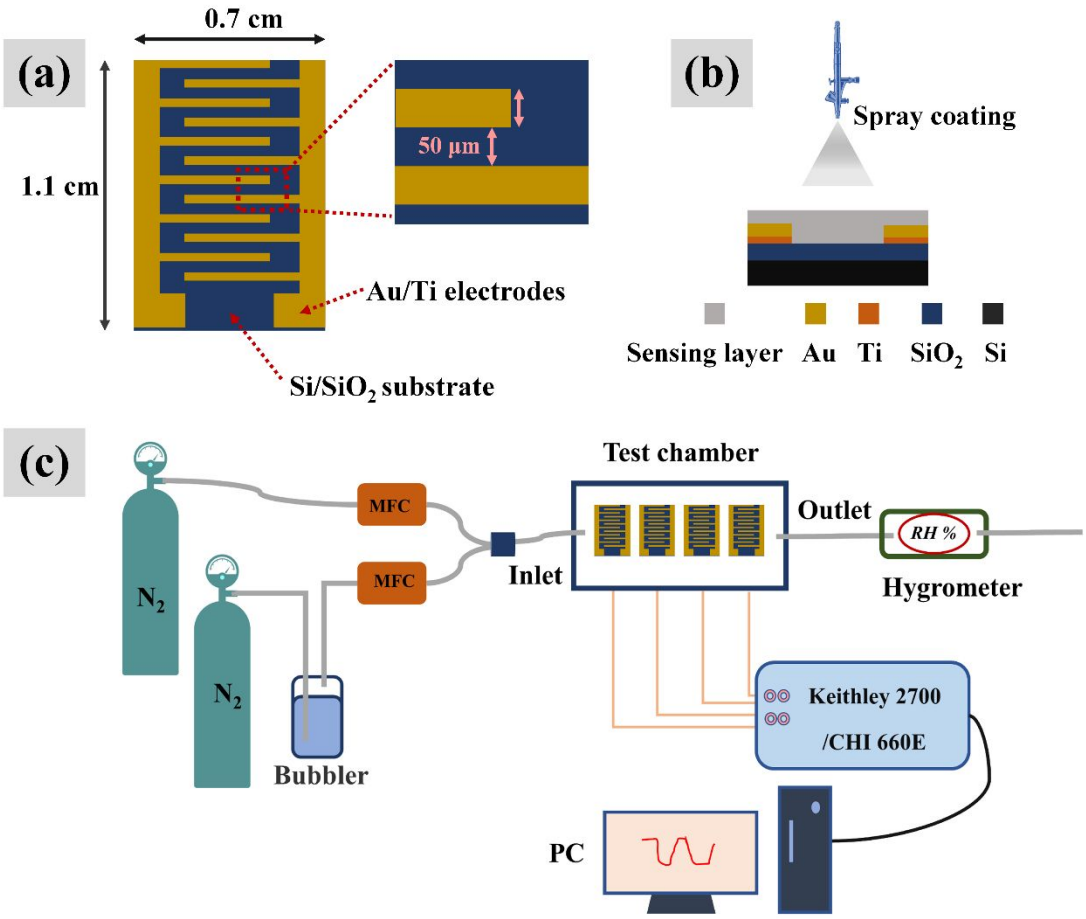

Figure S1. Schematic illustration of (a) IDEs device, (b) spray-coating and (c) measurement apparatus.

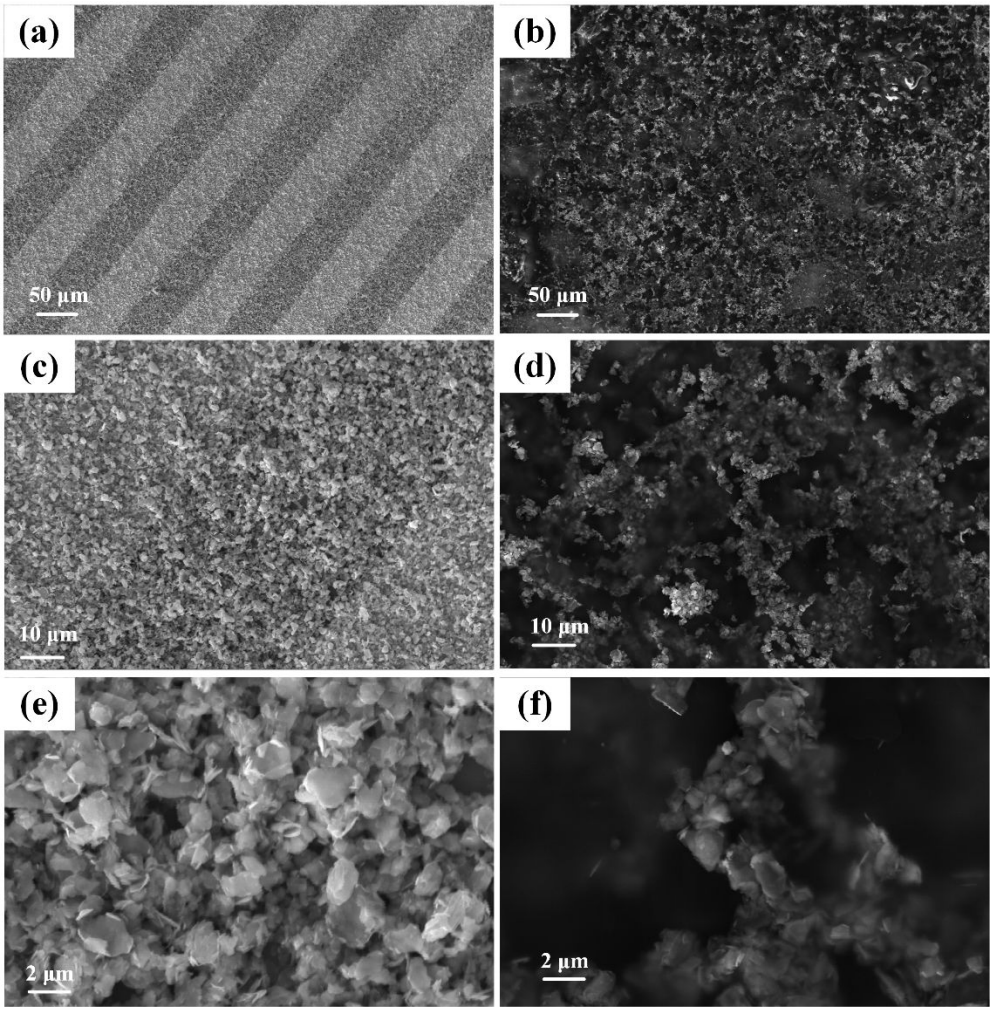

Figure S2. SEM images: gradual magnification of (a, c, e) MoS_2 and (b, d, f) MoS_2-PEO composite films.

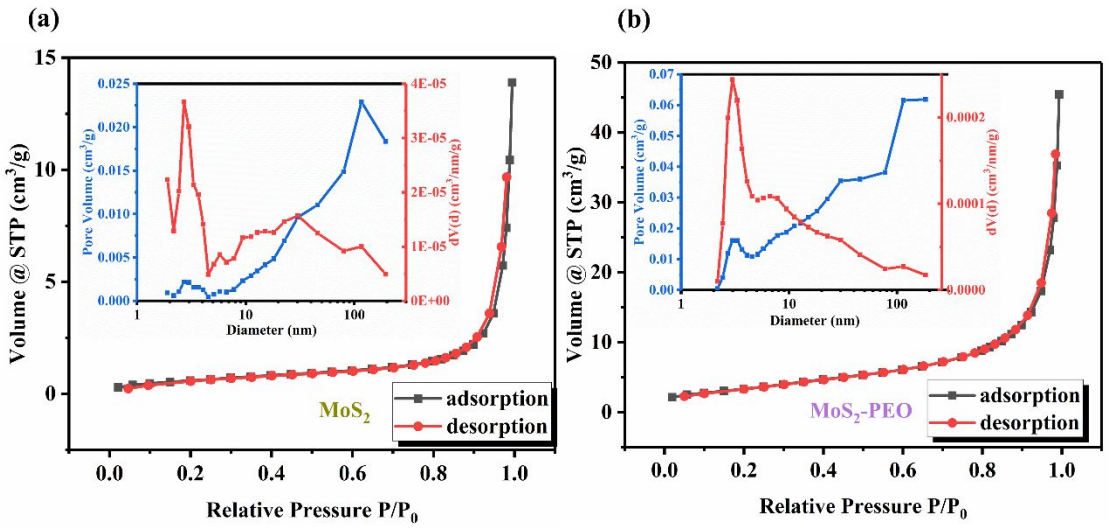

Figure S3. The adsorption/desorption isotherm, pore size distribution and pore volume of (a) MoS_2 and (b) MoS_2-PEO composites.

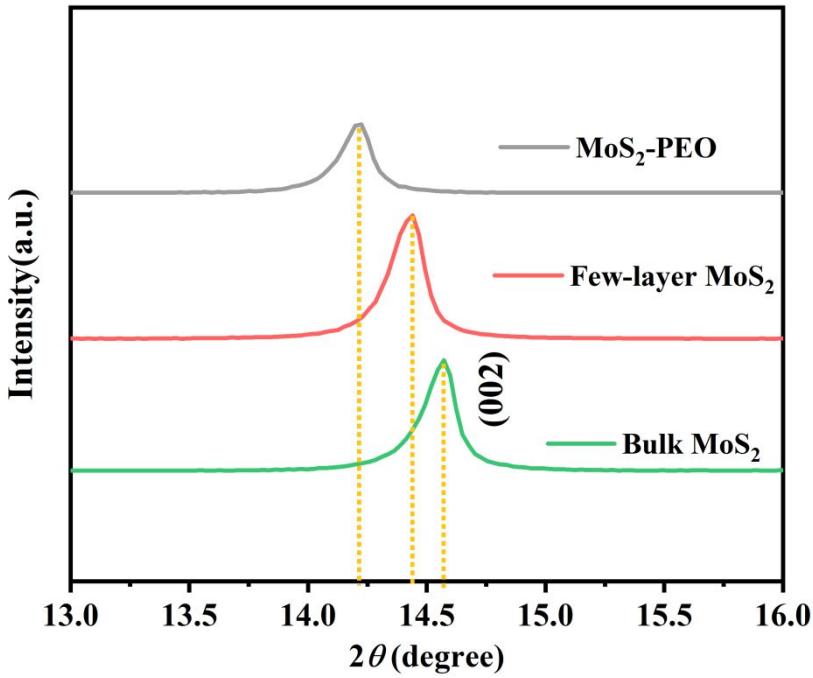

Figure S4. The downshift of (002) peak from bulk MoS_2, few-layer MoS_2 to MoS_2-PEO composites.

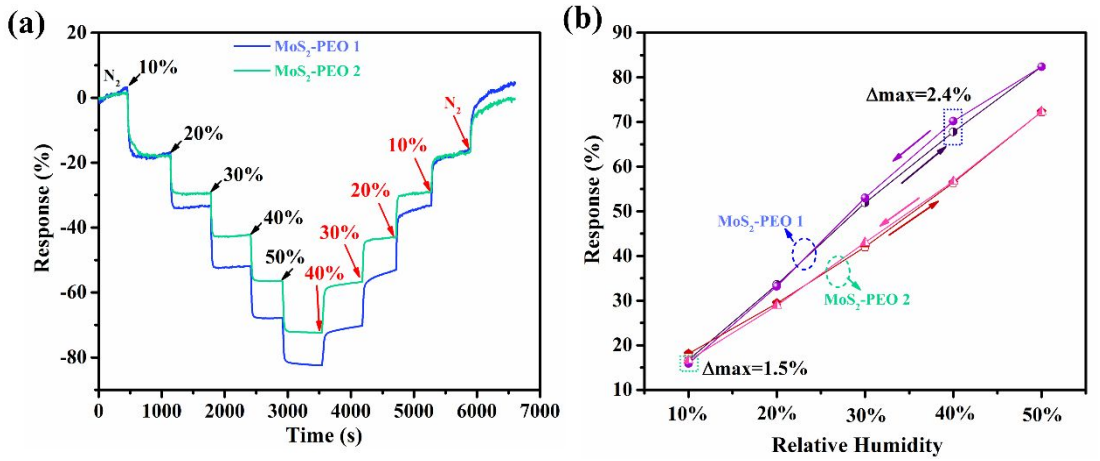

Figure S5. Response hysteresis of two different MoS_2-PEO sensors: (a) transient response and (b) response-RH relationship during the processes of ascending/descending RH.

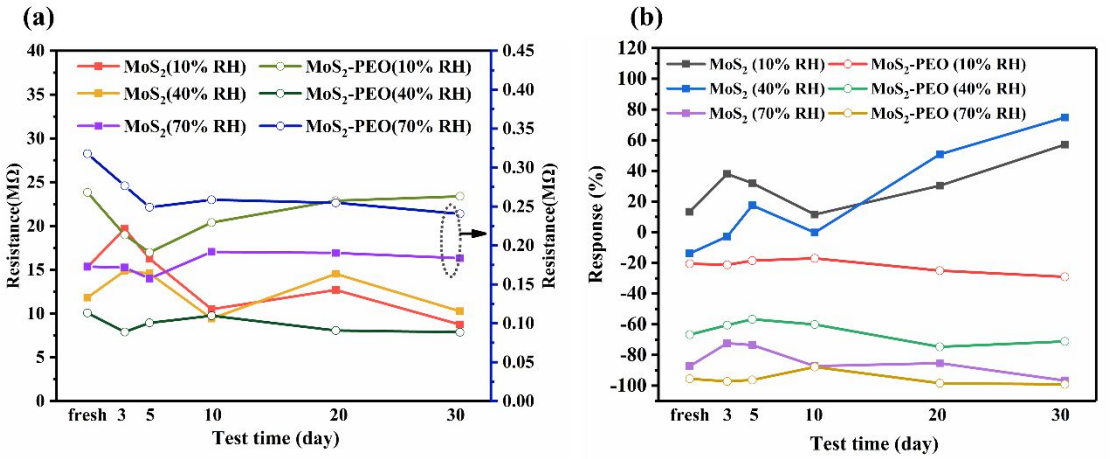

Figure S6. Operation stability of both MoS_2 and MoS_2-PEO sensors in terms of (a) saturation resistance and (b) response under different RH over time.

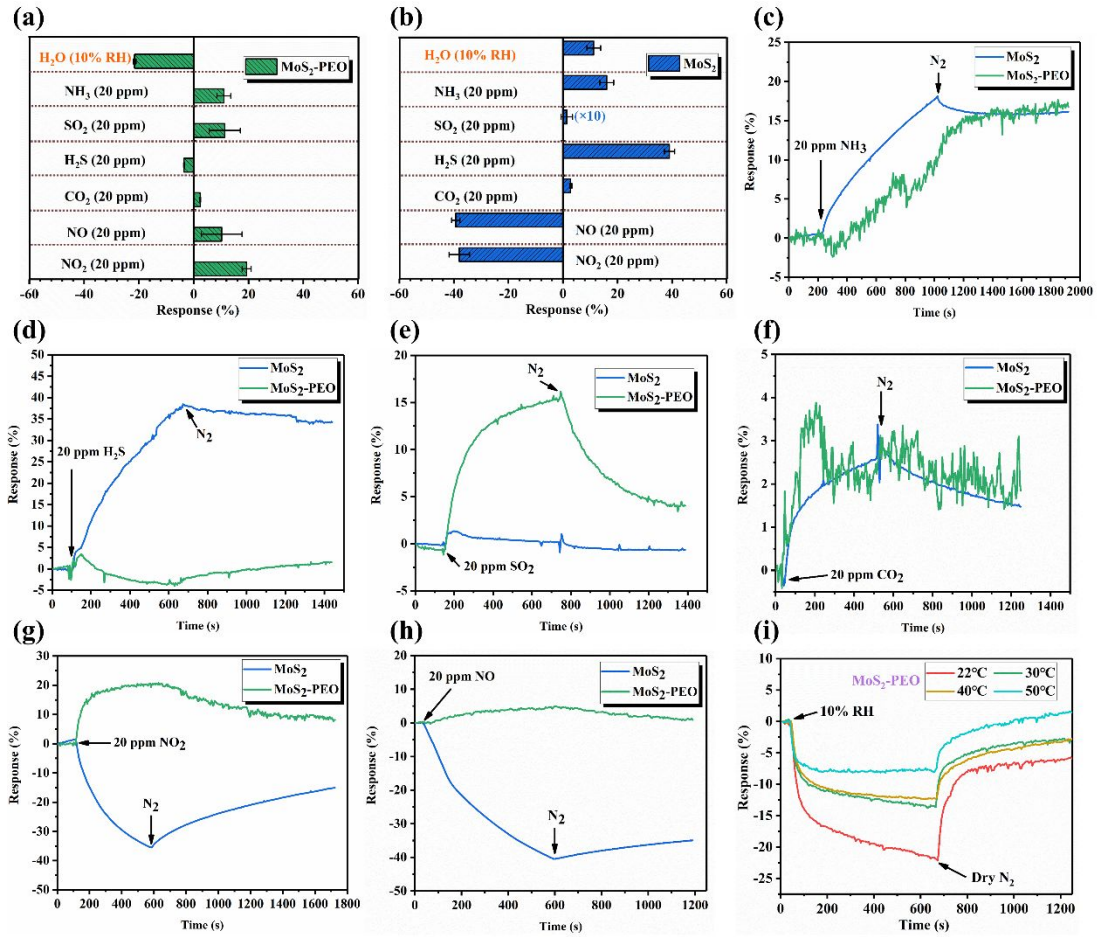

Figure S7. Selectivity of (a) MoS_2-PEO and (b) MoS_2 sensors, time-resolved response of both sensors toward (c) 20 ppm NH_3, (d) 20 ppm H_2S, (e) 20 ppm SO_2, (f) 20 ppm CO_2, (g) 20 ppm NO_2, and (h) 20 ppm NO_2 at room temperature, and (i) response transient of MoS_2-PEO sensor toward 10%RH at different operation temperature.

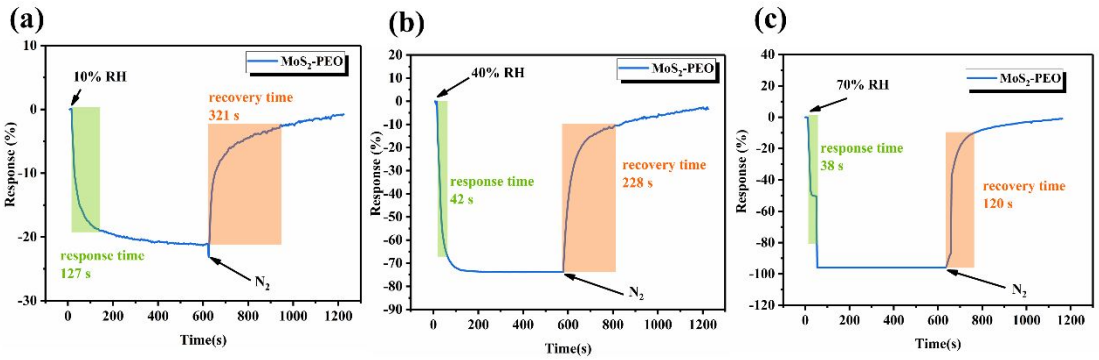

Figure S8. The response/recovery times of MoS_2-PEO sensor toward (a) 10%RH, (b) 40%RH, and (c) 70%RH.

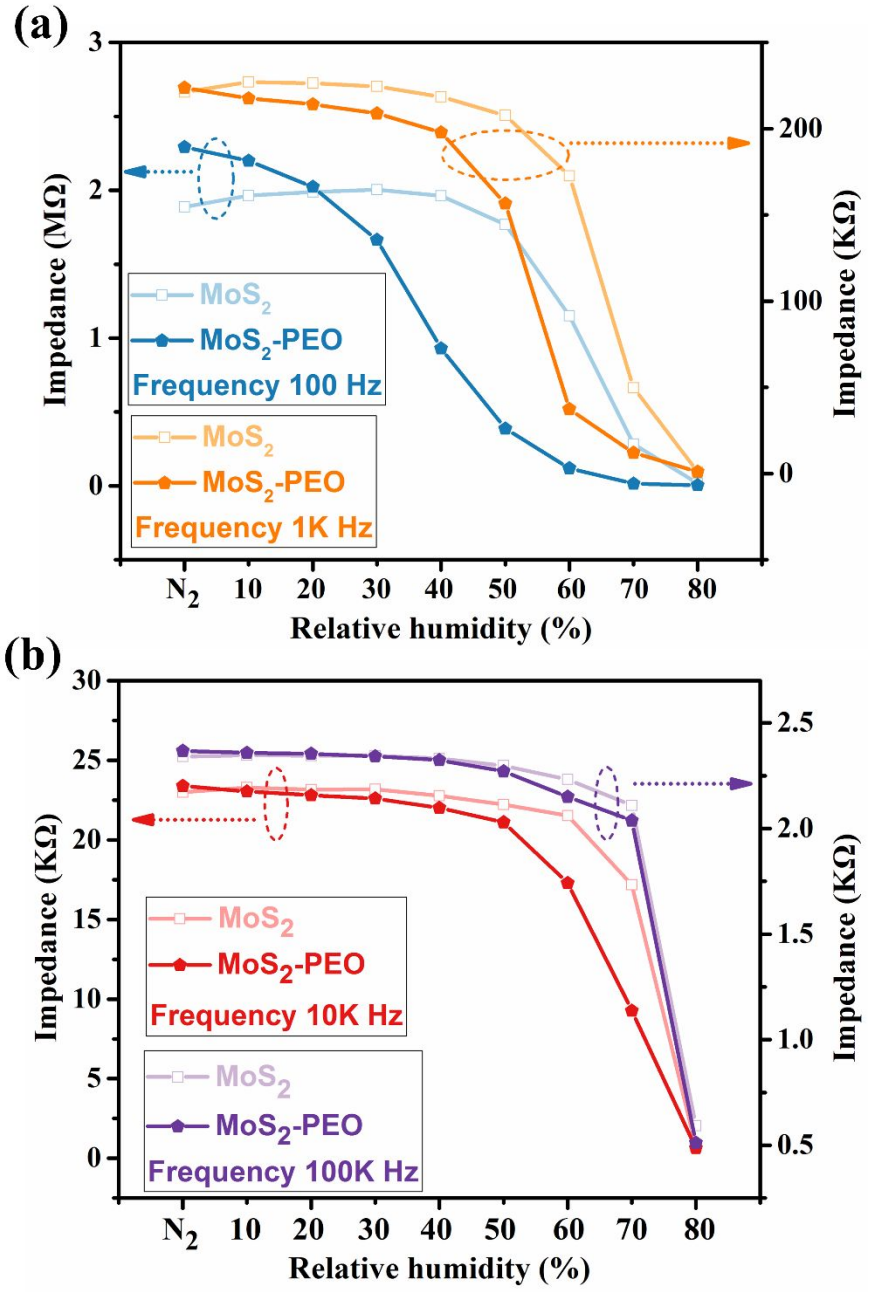

Figure S9. Impedance versus RH for MoS_2 and MoS_2-PEO sensors at (a) 100 Hz, 1K Hz, and (b) 10K Hz, 100K Hz.

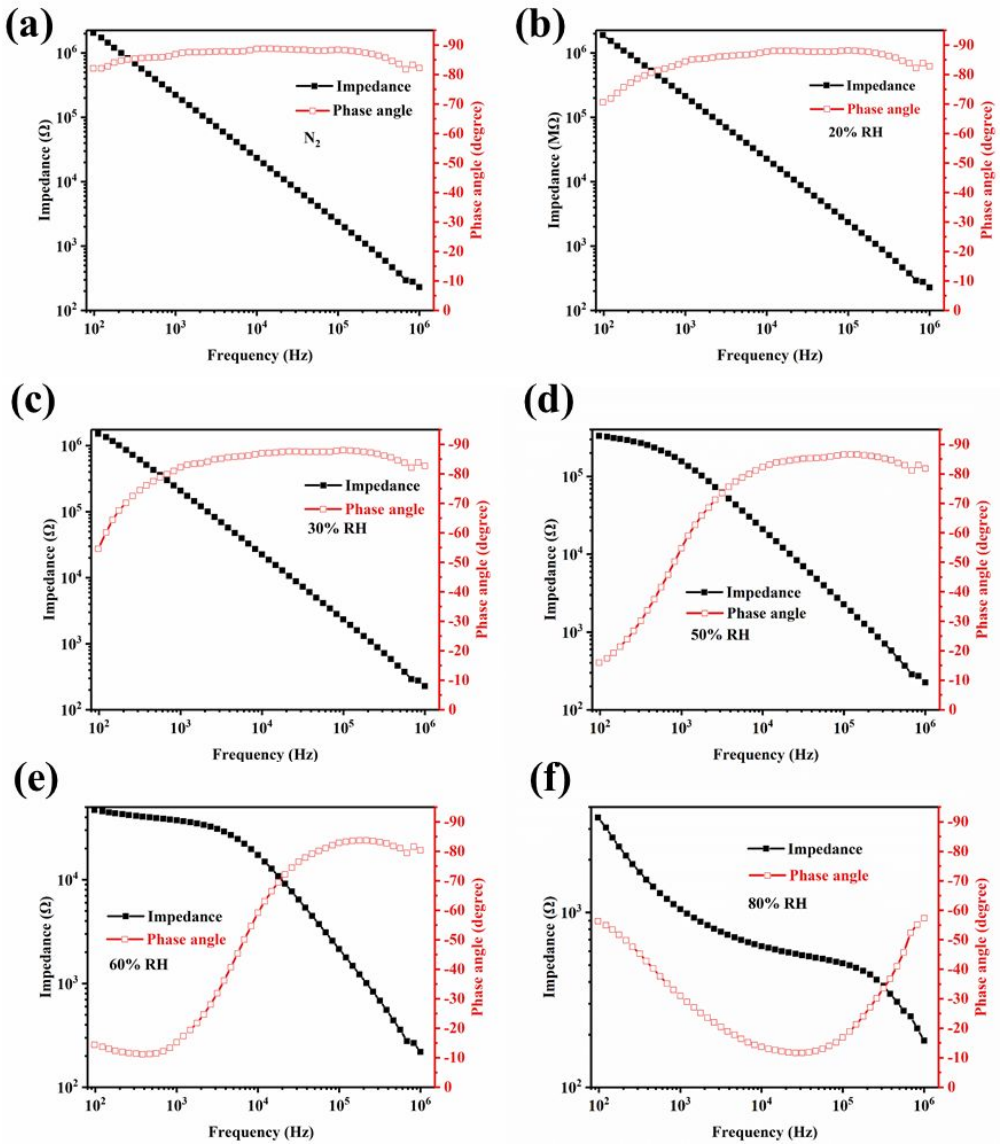

Figure S10. Bode plots of MoS_2-PEO sensor at (a) N_2, (b) 20%RH, (c) 30%RH, (d) 50%RH, (e) 60%RH and (f) 80%RH.

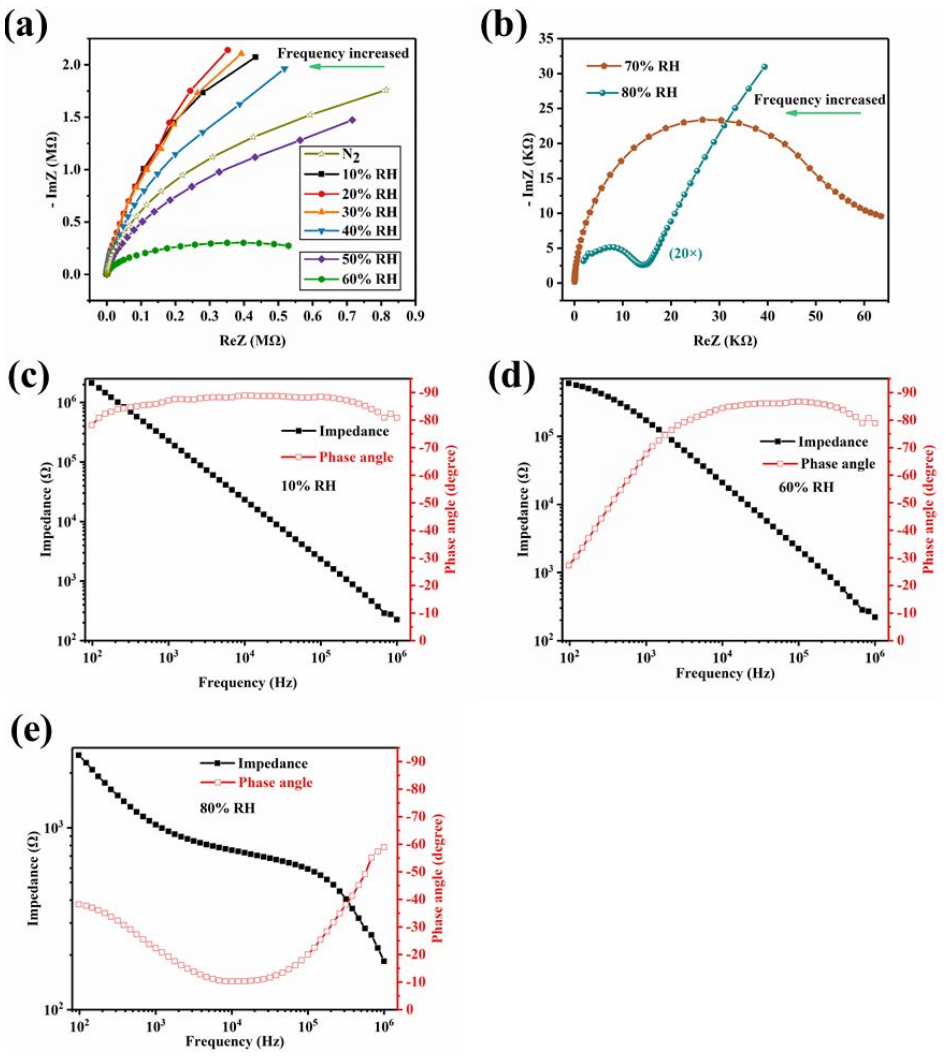

Figure S11. (a-b) CIS plots of MoS_2 sensor at different RH, bode plots of MoS_2 sensor at (c) 10%RH, (d) 60%RH and (e) 80%RH.

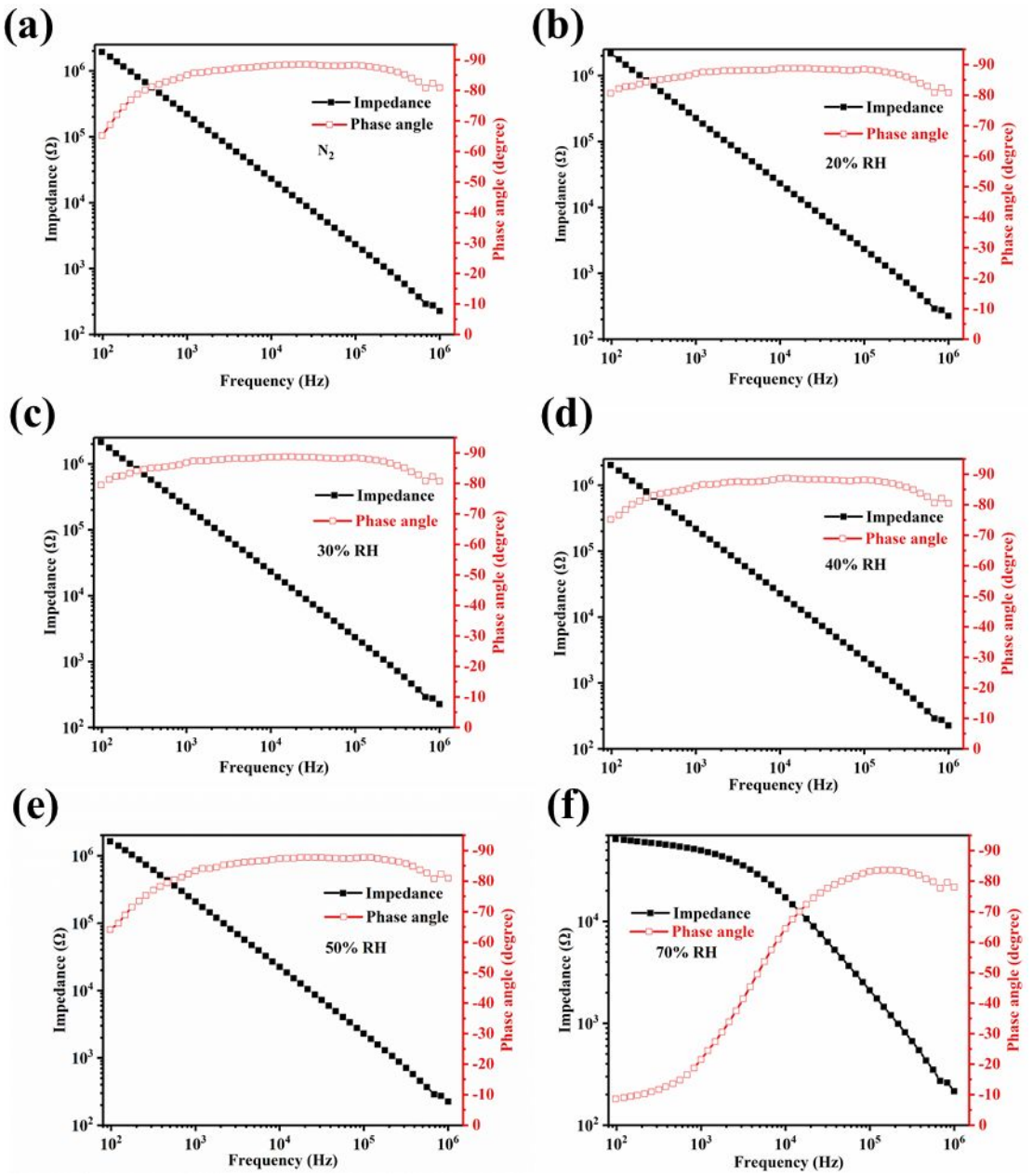

Figure S12. Bode plots of MoS_2 sensor at (a) N_2, (b) 20%RH, (c) 30%RH, (d) 40%RH, (e) 50%RH and (f) 70%RH.